Electronic Supplementary Information (ESI) file for the typescript entitled "Tautomeric and conformational switching in a new versatile N-rich heterocyclic ligand" by Emmanuele Parisi, Domenica Capasso, Amedeo Capobianco, Andrea Peluso, Sonia di Gaetano, Sandra Fusco, Carla Manfredi, Rosaria Mozzillo, Gabriella Pinto, and Roberto Centore

Synthesis of TT9

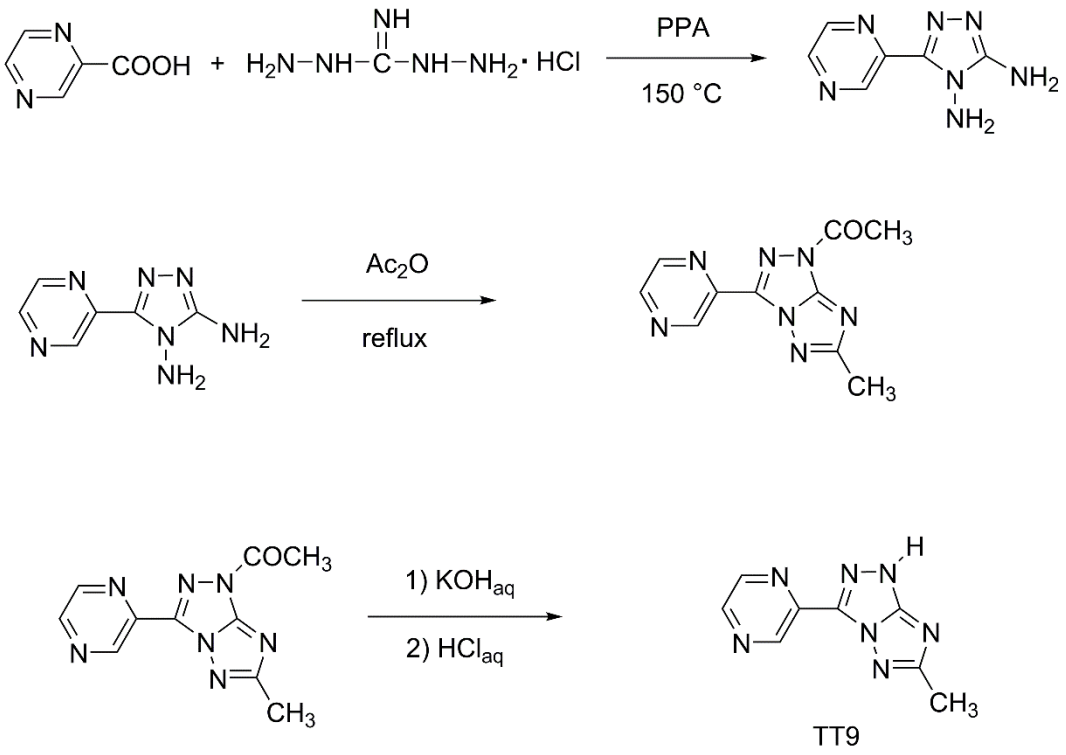

Scheme S1. Synthetic procedure for TT9.

NMR Spectra of 5-(2-pyrazinyl)-3,4-diamino-1,2,4-triazole

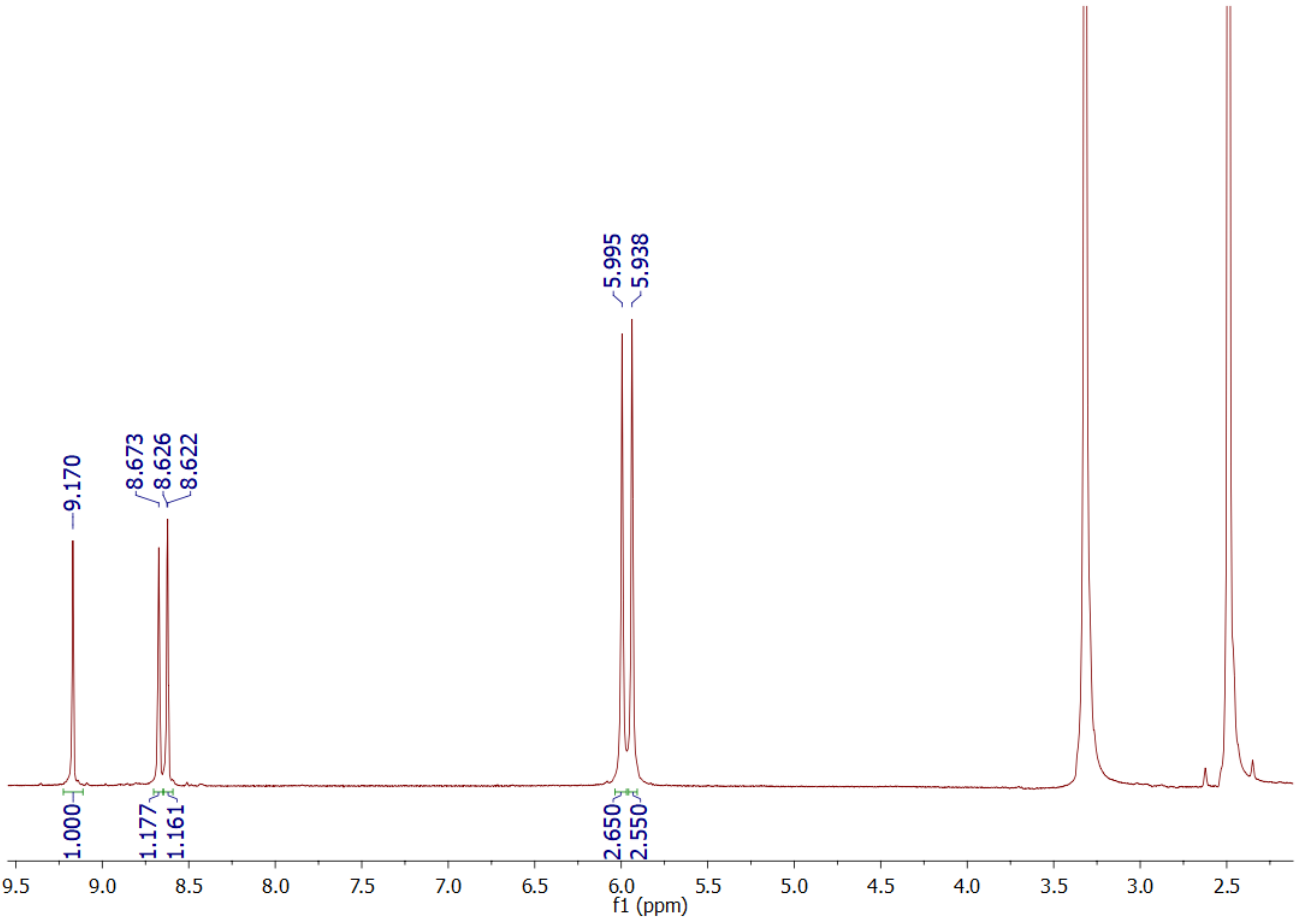

Fig. S1. ^{1}H-NMR spectrum of 5-(2-pyrazinyl)-3,4-diamino-1,2,4-triazole, in D6-DMSO, at 25 °C. The signals at 2.51 ppm and at 3.35 ppm are due to the solvent and water respectively.

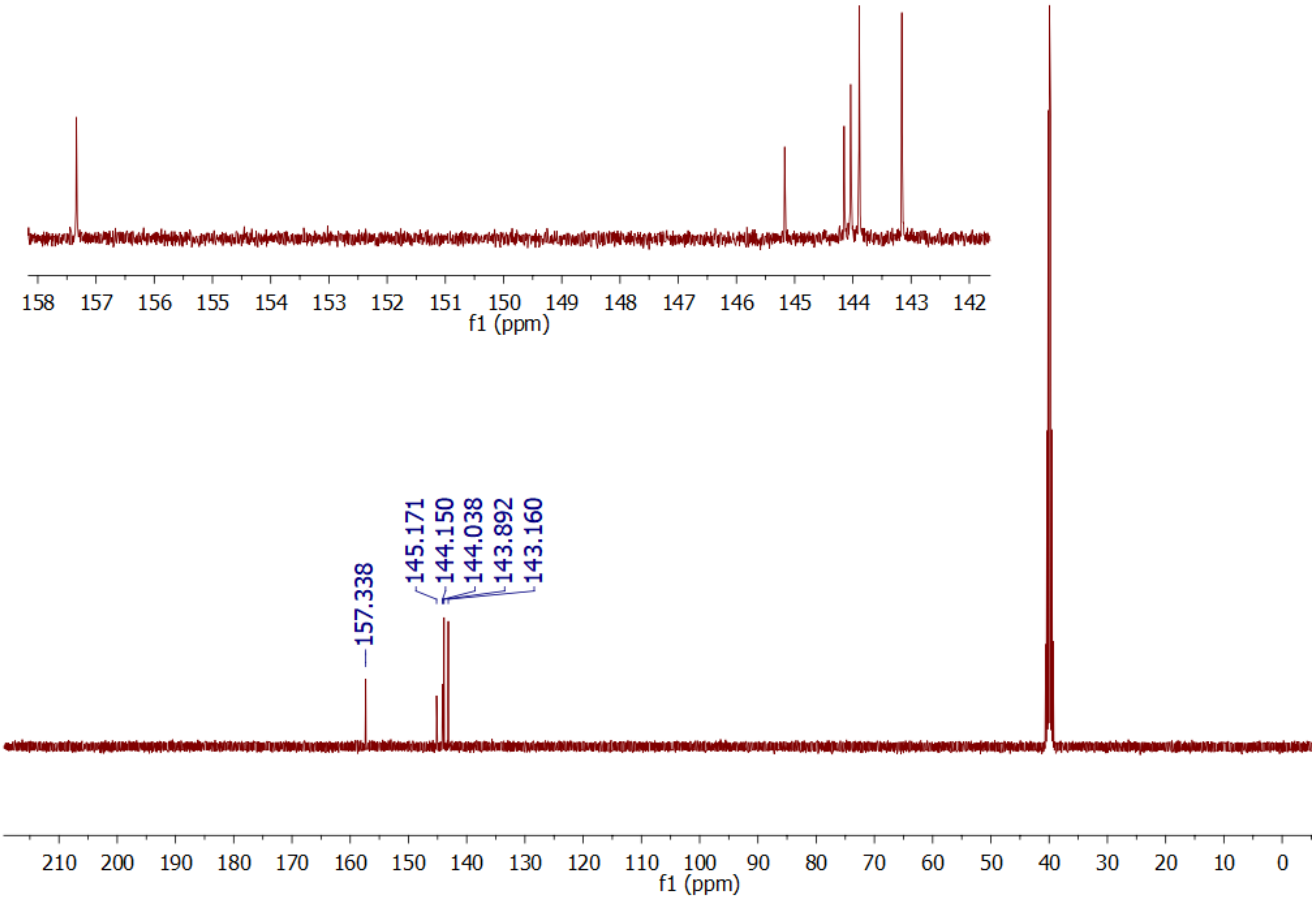

Fig. S2. ^{13}C-NMR spectrum of 5-(2-pyrazinyl)-3,4-diamino-1,2,4-triazole, in D6-DMSO, at 25 °C. The signals nearly 40 ppm are due to the solvent. In the inset, the region of the spectrum between 142 and 158 ppm has been expanded.

NMR Spectra of 4-methyl-7-(pyrazin-2-yl)-2H-[1,2,4]triazolo[3,2-c][1,2,4]triazole

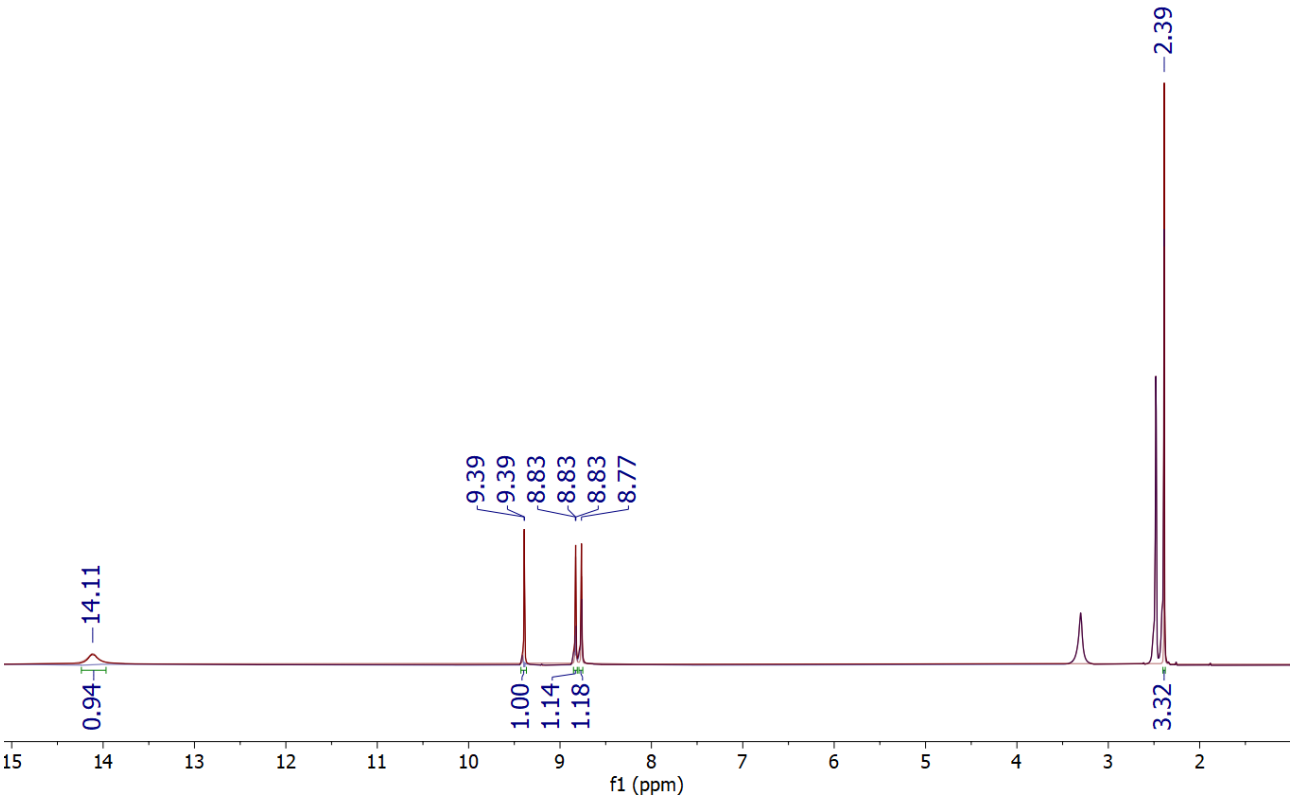

Fig. S3. ^{1}H-NMR spectrum of 4-methyl-7-(pyrazin-2-yl)-2H-[1,2,4]triazolo[3,2-c][1,2,4]triazole (TT9), in D6-DMSO, at 25 °C. The signals at 2.51 ppm and at 3.35 ppm are due to the solvent and water respectively.

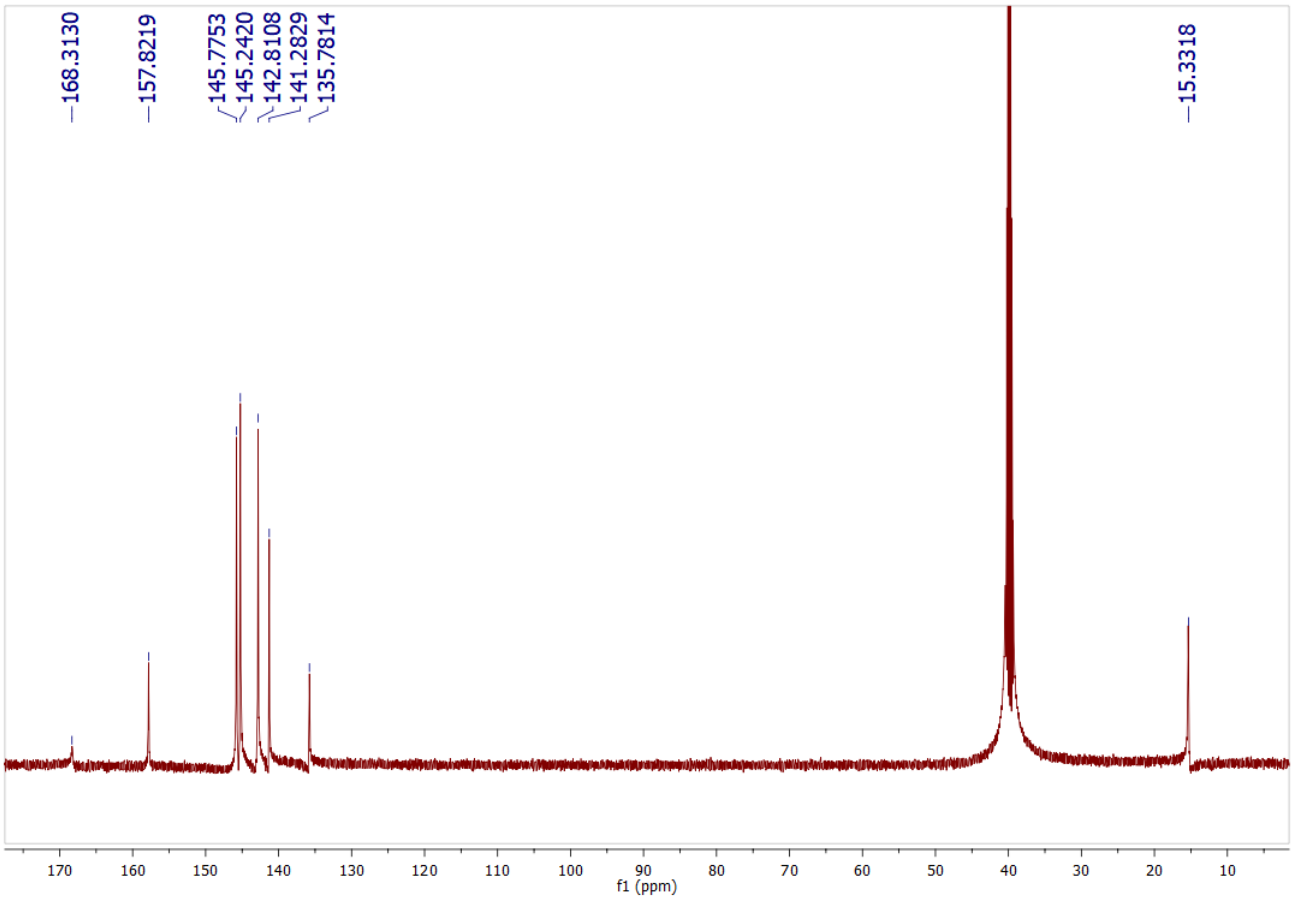

Fig. S4. ^{13}C-NMR spectrum of 4-methyl-7-(pyrazin-2-yl)-2*H*-[1,2,4]triazolo[3,2-c][1,2,4]triazole (TT9), in D6-DMSO, at 25 °C. The signals nearly 40 ppm are due to the solvent.

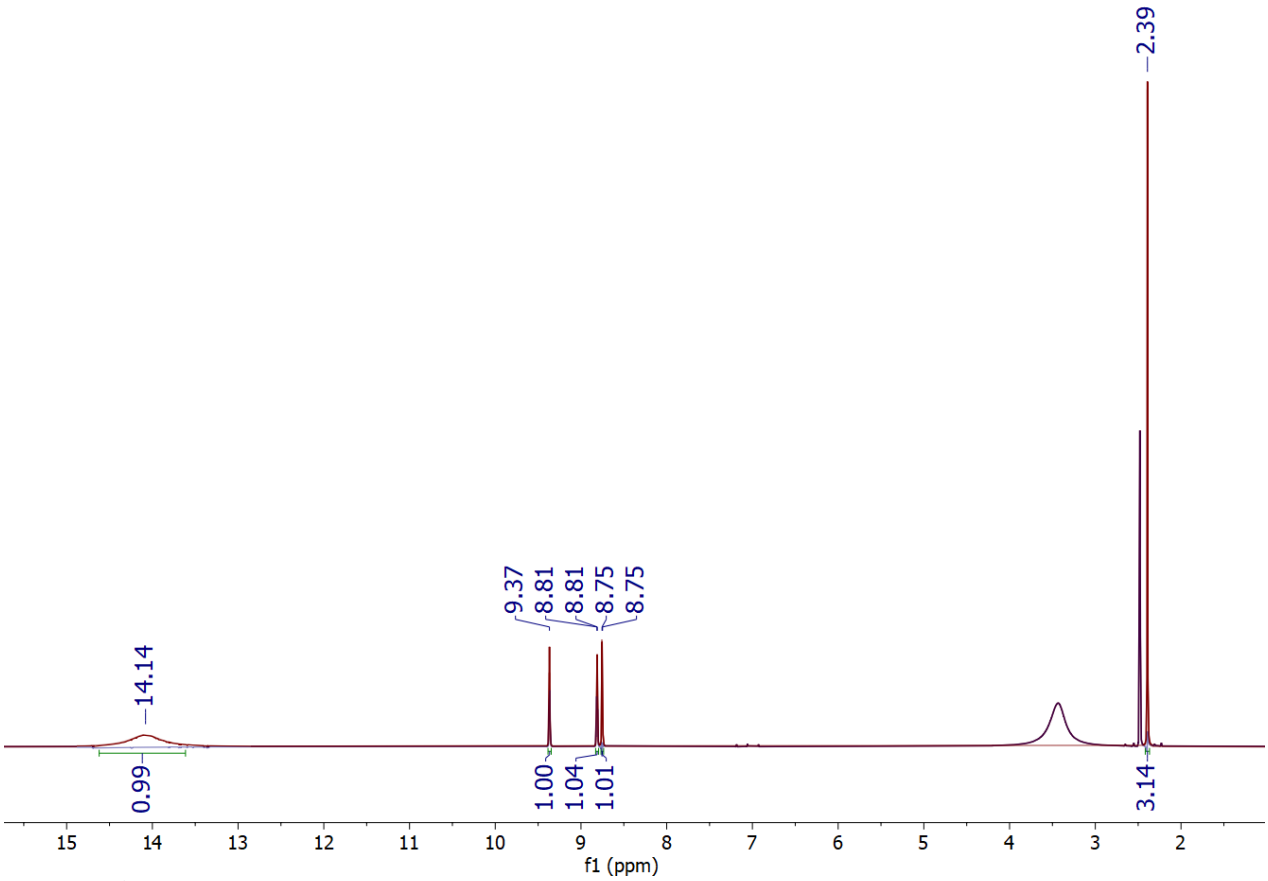

Fig. S5. ^{1}H-NMR spectrum of the complex $Zn_2(TT9)_2(H_2O)_6(Zn_2Br_6)_2 \cdot 2H_2O$, in D6-DMSO, at 25 °C. The signals at 2.51 ppm and at 3.35 ppm are due to the solvent and water respectively.

Mass Spectral Analysis

LC-MS/MS analysis

TT9 and the complex $Cu_2(TT9)_2Cl_4$ pentahydrate were dissolved in ethanol and Milli-Q water, respectively, at a concentration of 10 ppm useful for LC-MS/MS analysis by using a 6520 Accurate-Mass Q-TOF LC/MS system (Agilent Technologies) equipped with a 1200 HPLC system. After loading, the mixture (1 μL) was desalted at flow rate of 4 μL/min in a 40 nL enrichment column (Agilent Technologies chip) with 0.1% HCOOH as eluent. The sample was then loaded on a C18 reverse phase capillary column (75 μm*43 mm in the Agilent Technologies chip) at flow rate of 400 nL/min, with a linear gradient of eluent B (0.1% HCOOH in 95% acetonitrile) in A (0.1% HCOOH in 2% acetonitrile) from 5% to 50% in 20 min. The MS analysis was performed using a MS scan (mass range m/z 50−1000) followed by MS/MS scan scan (mass range m/z 20−1000) of the five most abundant ions in each MS scan. Mono-charged ions were preferably isolated and fragmented over singly charged ions. An error of 10 ppm was recorded for the standard mixture.

Results

A single elution peak was observed in the TIC chromatogram of both TT9 and Cu-TT9 solutions. Mass spectra of TT9 are shown in Fig. S6.

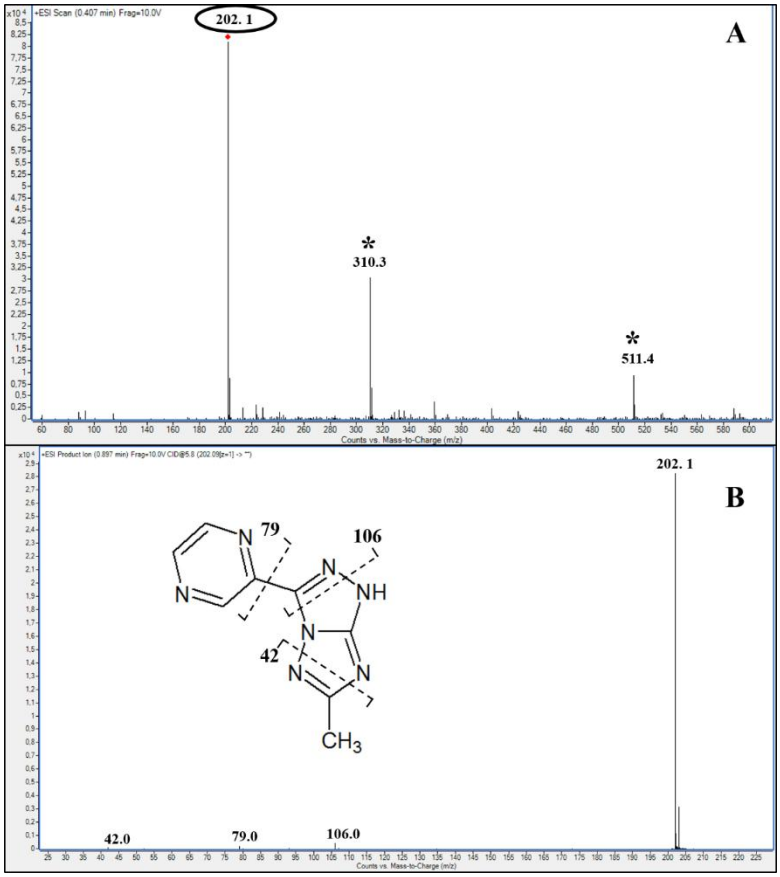

Fig. S6**.** MS spectrum under the TIC chromatogram of TT9 molecule (A). MS/MS spectrum of TT9 signal at 202.1 m/z (B). * indicate slip agents as plastic contaminants.

The MS spectrum under the peak showed a mass signal at 202.1 m/z (red circle) as the base peak together with other asterisked signals due to plastic contaminants (Fig. S6A). The MS/MS spectra confirmed the chemical structure of synthesized molecule, through the detection of fragment ions generated by collision in the reported regions (Fig. S6B). A signal at 106 m/z was attributed to pyrazine-2-carbonitrile as detected by others in a study of the synthesis of pyrazine derivatives.[1]

Another fragment ion derived by pyrazine was recorded in the MS/MS spectrum at 79 m/z probably attributable to the $[C_4H_3N_2]^+$ ion. A fragment at 42 m/z was instead identified as the $[CH_3–C{\equiv}N^+H]$ ion formed by the collision into the reported region (Fig. S6B).

The Cu-TT9 complex was also analyzed by LC-MS/MS enabling the confirmation of metal incorporation within the structure (Fig. S7).

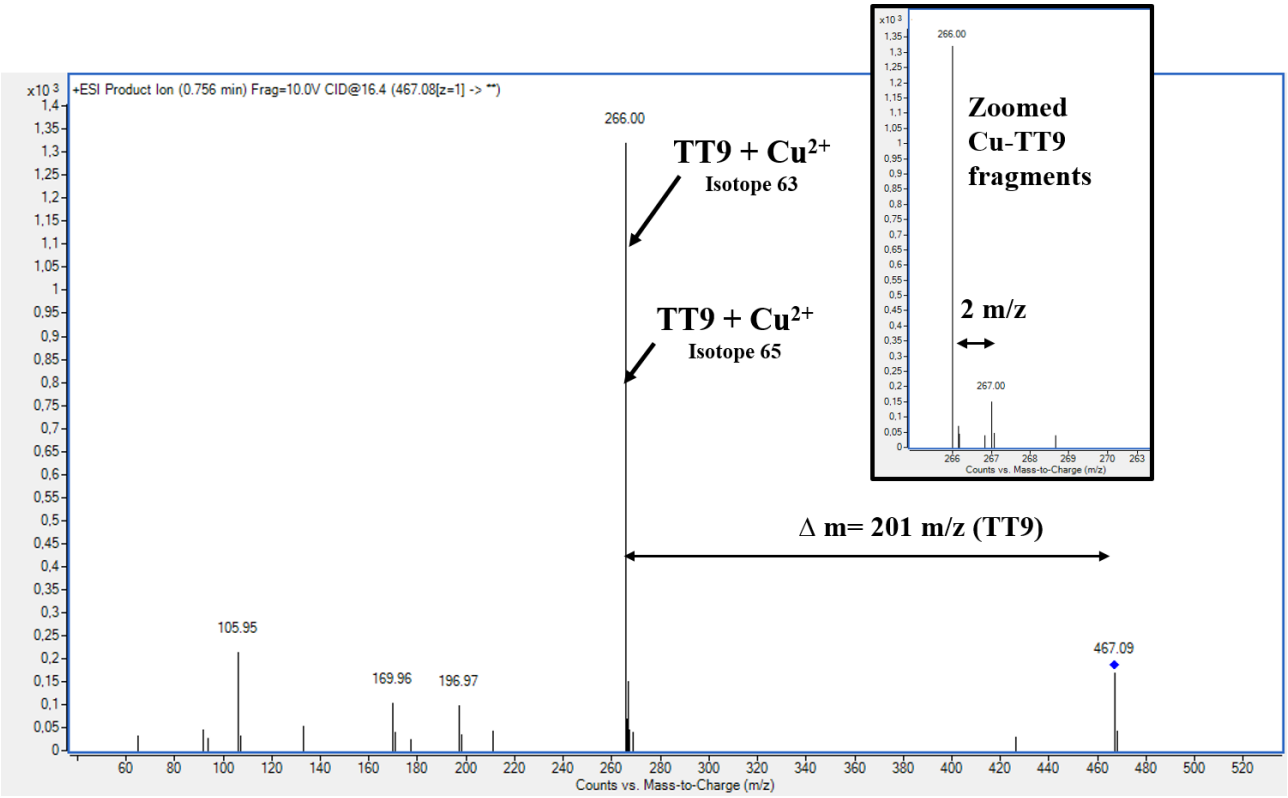

Fig. S7. MS/MS spectrum of Cu-TT9 complex.

The MS spectrum of solution containing Cu-TT9 complex showed a signal at 467.1 m/z that generated two fragments at 266 and 264 m/z in the MS/MS spectrum (Fig. S7). The delta shift of 2 m/z confirmed the presence of two Cu isotopes (63 and 65 Da) showing the natural abundance of 69% and 31%, respectively, as reported in the zoomed insert of Fig. S7. Interestingly, the precursor ion at 467 m/z indicates that, in the conditions in which the MS is measured, the cationic complex contains two TT9 ligand molecules and one Cu^{2+} ion (Fig. S7), which is a different result as compared with the analysis in solution reported in the typescript. By fragmentation of this $Cu(TT9)_2^{2+}$ complex, the complex $Cu(TT9)^{2+}$ is obtained. The fragment at 106 m/z attributed to the pyrazine-2-carbonitrile

in the MS/MS spectrum of TT9 molecule (Fig. S6B) was also generated by fragmentation of Cu-TT9 complex (Fig. S7).

Full computational results

In Tab. S1 are reported the computed energies of the tautomers of neutral TT9, in gas phase and in water. The last two entries in the Table refer to the case in which the H atom is on the *ortho* nitrogen of the pyrazinic ring, see Scheme S2.

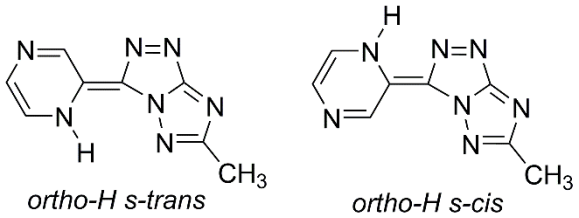

Scheme S2. Tautomer-conformers of neutral TT9 with the H atom bonded to the *ortho* N atom of pyrazinic ring.

Table S1. Relative energies (BMK/6-31+G**, kcal/mol, include ZPVE) of the tautomers/conformers of TT9.

Tautomer/conformer	Gas	Water
1*H s-trans*		+7.2
1*H s-cis*		+3.5
2*H s-trans*	+0.6	+0.1
2*H s-cis*	**0.0**	**0.0**
3*H s-trans*	+6.5	+1.4
3*H s-cis*	+8.6	+1.9
5*H s-trans*	+12.7	+7.8
5*H s-cis*	+22.7	+13.3
ortho-H s-trans		+12.6
ortho-H s-cis		+13.4

The computed energies of tautomers of singly protonated TT9 are reported in Tab. S2. In this case, we have considered all the possibilities, including those in which one or both N-H protons are on N atoms of the pyrazinic ring. The total number of tautomers can be calculated considering that there are two H atoms and six possible N atoms (four on the triazolo-triazole and two on pyrazine), hence the number of tautomers is

$$\binom{6}{2} = \frac{6!}{2! \cdot 4!} = 15$$

However, for each tautomer there are two conformational isomers (*s-cis* and *s-trans*), so the total number of tautomers/conformers is 30.

In the entries of Tab. S2, the protonated N atoms of the pyrazinic ring are indicated as *meta* or *ortho*. Two examples of tautomers/conformers in which one H atom is bonded to N atoms of the pyrazinic ring are reported in Scheme S3.

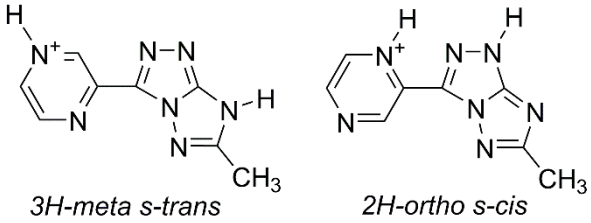

Scheme S3. Two tautomer-conformers of singly protonated TT9 in which one H atom is bonded to the *meta* or *ortho* N atom of pyrazinic ring.

Table S2. Relative energies (BMK/6-31+G**, kcal/mol, include ZPVE) of the tautomers/conformers of singly protonated TT9.

Tautomer/conformer	Gas	Water
1*H*-2*H s-cis*	19.0	14.5
1*H*-2*H s-trans*	27.5	18.7
1*H*-3*H s-cis*	**0.0**	**0.0**
1*H*-3*H s-trans*	6.2	3.2
1*H*-5*H s-cis*	16.8	12.3
1*H*-5*H s-trans*	13.6	9.4
1*H-meta s-cis*	23.6	10.0
1*H-meta s-trans*	34.9	14.2
1*H-ortho s-cis*	33.2	18.1
1*H-ortho s-trans*	24.5	14.4
2*H*-3*H s-cis*	**9.3**	**1.7**
2*H*-3*H s-trans*	**7.5**	**1.1**
2*H*-5*H s-cis*	16.7	10.6
2*H*-5*H s-trans*	5.2	4.4
2*H-meta s-cis*	14.0	4.7
2*H-meta s-trans*	15.7	4.6
2*H-ortho s-cis*	12.1	6.6
2*H-ortho s-trans*	9.4	5.9
3*H*-5*H s-cis*	39.3	20.3
3*H*-5*H s-trans*	25.3	13.2
3*H-meta s-cis*	16.9	5.0
3*H-meta s-trans*	**13.0**	**4.1**
3*H-ortho s-cis*	8.6	4.8
3*H-ortho s-trans*	10.9	5.0
5*H-meta s-cis*	40.5	18.5
5*H-meta s-trans*	25.8	11.4
5*H-ortho s-cis*	28.3	17.2
5*H-ortho s-trans*	36.3	20.0
meta-ortho s-cis	45.8	26.4
meta-ortho s-trans	42.7	24.6

Table S3. Relative energies (BMK/6-31+G**, kcal/mol, include ZPVE) of the tautomers/conformers of doubly protonated TT9.[a]

Tautomer/conformer	Gas	Water
1*H*-2*H*-3*H s-cis*	32.3	21.1
1*H*-2*H*-3*H s-trans*	39.8	24.9
1*H*-2*H*-5*H s-cis*	41.6	31.1
1*H*-2*H*-5*H s-trans*	38.7	27.8
1*H*-2*H*-6*H s-cis*	48.6	30.5
1*H*-2*H*-6*H s-trans*	40.7	27.6
1*H*-2*H*-7*H s-cis*	27.4	18.6
1*H*-2*H*-7*H s-trans*	38.3	22.8
1*H*-3*H*-5*H s-cis*	35.6	22.4
1*H*-3*H*-5H *s-trans*	28.7	18.1
1*H*-3*H*-7*H s-cis*	2.9	1.3
1*H*-3*H*-7*H s-trans*	10.3	4.9
1*H*-5*H*-7*H s-cis*	28.9	15.2
1*H*-5*H*-7*H s-trans*	25.4	12.4
2*H*-3*H*-5*H s-cis*	48.8	25.9
2*H*-3*H*-5*H s-trans*	32.8	17.9
2*H*-3*H*-6*H s-cis*	7.2	4.4
2*H*-3*H*-6*H s-trans*	8.8	4.8
2*H*-3*H*-7*H s-cis*	2.5	0.6
2*H*-3*H*-7*H s-trans*	**0.0**	**0.0**
2*H*-5*H*-7*H s-cis*[b]	–	11.8
2*H*-5*H*-7*H s-trans*	6.3	4.9
3*H*-5*H*-7*H s-cis*[b]	–	19.7
3*H*-5*H*-7*H s-trans*	18.5	12.2

[a] N6 and N7 are, respectively, *ortho* and *meta* N atoms of the pyrazine ring. [b] the *s-cis* conformation goes to *s-trans* during gas phase optimization, while it is kept in the optimization in water.

The total number of tautomers can be calculated considering that there are three H atoms and six possible N atoms (four on the triazolo-triazole and two on pyrazine), hence the number of tautomers is

$$\binom{6}{3} = \frac{6!}{3! \cdot 3!} = 20$$

Again, for each tautomer there are two conformational isomers (*s-cis* and *s-trans*), so the total number of tautomers/conformers would be 40. However, based on the results for the neutral and singly protonated species, we have ruled out tautomers/conformers in which there are two protons on the pyrazine ring.

Acid-base equilibria, UV-VIS spectra, UV-VIS titrations and distribution diagrams

In this section, TT9 will also be indicated as *HL*, the singly protonated form of TT9 as H_2L^+, and the deprotonated form as L^-. The protolytic equilibria of TT9 were studied by UV-Vis absorption spectroscopy in 0.5 M NaCl - 4 % ethanol (v/v), as the ionic medium. The TT9 stock solutions in 100 % ethanol were prepared starting from the solid. Deionized and doubly distilled water was used to prepare all aqueous solutions. NaCl (Fluka, dried overnight at 120 °C) was used to prepare the ionic medium solutions. Stock solutions of HCl (Carlo Erba p.a.) were standardized against $KHCO_3$ using methyl red as indicator, with a reproducibility of 0.1 %. NaOH (Baker p.a.) stock solutions were standardized against standardized HCl solutions. The experiments were performed as acid-base titrations at constant total concentration of TT9 (C= $3.0 \cdot 10^{-5}$ M). The investigated pH spans between 0.3 and 12. For each experimental point at 2.5<pH<10, the equilibrium free proton concentration was evaluated from the measured electromotive force at the ends of the galvanic cell GE/TS/RE, where TS indicates the Test solution, GE is the glass electrode and RE is a reference electrode (0.5 M NaCl|Hg_2Cl_2|Hg(Pt)) placed outside but electrically connected to TS through a salt bridge. The Nernst potential of the cell, E(mV), can be written as $E = E_0 + 59.16 \log [H^+] + E_j$ where E_j= liquid junction potential due to the replacement of Na^+ with H^+.[2] The evaluation of the constant of the glass electrode, E_0, was performed in the first stage of each experiment by a coulometric titration, using the Gran method.[3] All the test solution at 0.3<pH<2 were obtained analytically. Formation of complexes of TT9 with Cu^{2+} and Zn^{2+} was investigated by UV–vis spectrophotometry, as well. The experiments were performed as acid–base titrations of TT9–Cu(II) or TT9-Zn(II) solutions, keeping constant the total concentration of the triazole (C= $3.0 \cdot 10^{-5}$ M) and of the metal, at various metal/ligand concentration ratios (1/1, 1/2, 1/4). The pH range investigated was 3<pH<7 for TT9-Cu(II) and 1<pH<10 for TT9-Zn(II). The upper limit of pH is imposed by precipitation of sparingly soluble metal hydroxides. All the experiments were carried out in air in a thermostat, at 25.00 ± 0.03 °C. Potentiometric experimental data were collected by means of an automatic data acquisition system based on Hewlett-Packard (HP) instrumentation. The glass membrane electrodes reversible to protons were supplied by Metrohm. Highly precise (± 0.02 mV) emf measurements were made by adapting the impedance of the glass electrode through operational amplifiers. Coulometric variations of the solution composition were carried out using a Hewlett Packard "DC Power Supply". The intensity of the current in the electrolysis circuit was measured from the potential drop at the ends of a calibrated resistance; the current density was set at about 1 mA/cm^2. Absorption spectra were recorded with a Varian Cary 50 UV-Vis spectrophotometer using 1 cm cell. The primary spectrophotometric data (Absorbance, pH, λ) were elaborated both graphically and numerically, by the HYPERQUAD program.[4] In particular, in Figures S9 and S12, the continuous curves were obtained by fitting the

experimental points with an equation that relates the Absorbance of the solution (at a given wavelength) with the pH, the analytical concentration of TT9, and the equilibrium constants, by assuming the law of additivity of absorbances (Bouger-Lambert-Beer equation). In the case of the complexation equilibria, the analytical concentration of the metal and the stability constants of the complexes, must also be included in the Bouger-Lambert-Beer equation. The Bouger-Lambert-Beer equation is derived below for the system TT9 (HL).

From the Lambert-Beer law, assuming additivity of the absorbances, it is

$$A^{\lambda} = b\left(\sum_i \varepsilon_i^{\lambda} c_i\right) = b\left(\varepsilon_1^{\lambda}[H_2L^+] + \varepsilon_2^{\lambda}[HL] + \varepsilon_3^{\lambda}[L^-]\right) \quad (1)$$

in which b is the optical path of the cell (1 cm) and ε_i^{λ} is the molar extinction coefficient of the species i at the given wavelength. The analytical concentration of TT9 (HL), C, is given by

$$C = [H_2L^+] + [HL] + [L^-] \quad (2)$$

The acid-base conditional equilibrium constants are

$$K_{a1} = \frac{[HL]\cdot[H_3O^+]}{[H_2L^+]}, K_{a2} = \frac{[L^-]\cdot[H_3O^+]}{[HL]} \quad (3)$$

From these, it is possible to express the concentration of each species but one (e. g. the neutral one), as a function of the equilibrium constants and the concentration of H_3O^+:

$$[H_2L^+] = \frac{[HL]\cdot[H_3O^+]}{K_{a1}}, [L^-] = \frac{[HL]\cdot K_{a2}}{[H_3O^+]} \quad (4)$$

Putting (4) in (2) it is

$$C = \frac{[HL]\cdot[H_3O^+]}{K_{a1}} + [HL] + \frac{[HL]\cdot K_{a2}}{[H_3O^+]} \quad (5)$$

So, it is

$$[HL] = \frac{CK_{a1}[H_3O^+]}{[H_3O^+]^2 + K_{a1}[H_3O^+] + K_{a1}K_{a2}} \quad (6)$$

Putting (4) and (6) in (1) yields

$$A = b\cdot\left(\varepsilon_1^{\lambda}\frac{[HL]\cdot[H_3O^+]}{K_{a1}} + \varepsilon_2^{\lambda}[HL] + \varepsilon_3^{\lambda}\frac{[HL]\cdot K_{a2}}{[H_3O^+]}\right) \quad (7)$$

$$A = b\cdot[HL]\left(\varepsilon_1^{\lambda}\frac{[H_3O^+]}{K_{a1}} + \varepsilon_2^{\lambda} + \varepsilon_3^{\lambda}\frac{K_{a2}}{[H_3O^+]}\right) \quad (8)$$

$$A = b\cdot\frac{CK_{a1}[H_3O^+]}{[H_3O^+]^2 + K_{a1}[H_3O^+] + K_{a1}K_{a2}}\left(\varepsilon_1^{\lambda}\frac{[H_3O^+]}{K_{a1}} + \varepsilon_2^{\lambda} + \varepsilon_3^{\lambda}\frac{K_{a2}}{[H_3O^+]}\right) \quad (9)$$

$$A = b \cdot \frac{C}{[H_3O^+]^2 + K_{a1}[H_3O^+] + K_{a1}K_{a2}} \left(\varepsilon_1^\lambda [H_3O^+]^2 + \varepsilon_2^\lambda K_{a1}[H_3O^+] + \varepsilon_3^\lambda K_{a1}K_{a2}\right) \quad (10)$$

and, finally, the Bouger-Lambert-Beer equation

$$A = b \cdot \frac{C}{10^{-2pH} + 10^{-pH-pK_{a1}} + 10^{-pK_{a1}-pK_{a2}}} \left(\varepsilon_1^\lambda 10^{-2pH} + \varepsilon_2^\lambda 10^{-pH-pK_{a1}} + \varepsilon_3^\lambda 10^{-pK_{a1}-pK_{a2}}\right)$$

The UV-VIS spectra, at constant total concentration and different pH, are reported in Fig. S8 for TT9.

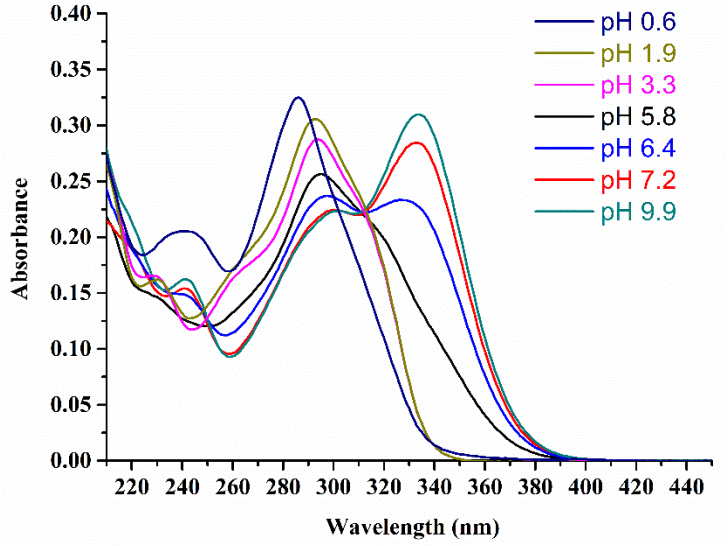

Fig. S8. UV−VIS absorption spectra of TT9 at constant total concentration, C = 3.0 × 10^{-5} M, in NaCl 0.5 M/ethanol 4% (v/v) recorded at 0.6 ≤ pH ≤ 9.9.

The plots of Absorbance *vs* pH at fixed wavelength and the fitting of the points using the Bouger-Lambert-Beer equation are reported in Fig. S9.

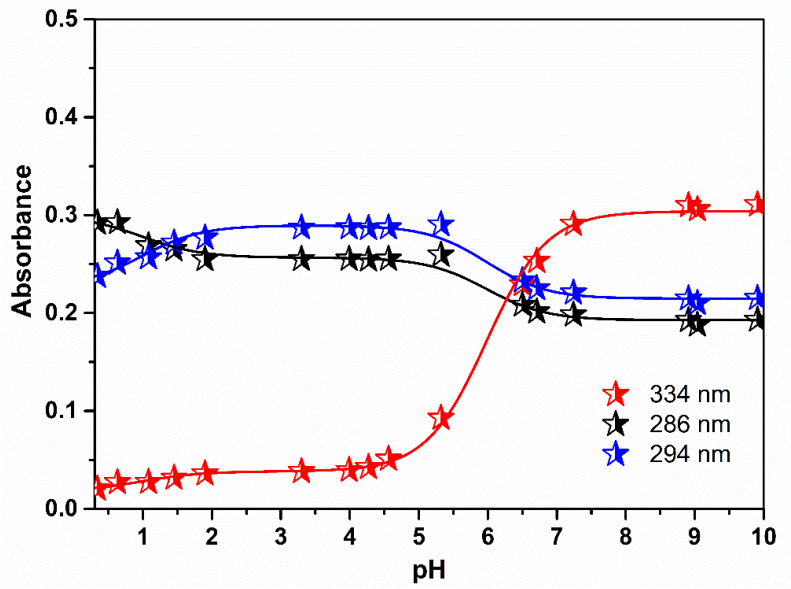

Fig. S9. UV-VIS titration curves of TT9, at four different wavelengths. The continuous curves have been constructed by fitting the experimental points (absorbance vs pH data taken from Fig. S7) with the Bouger-Lambert-Beer equation.

The distribution diagram of TT9 is shown in Fig. S10.

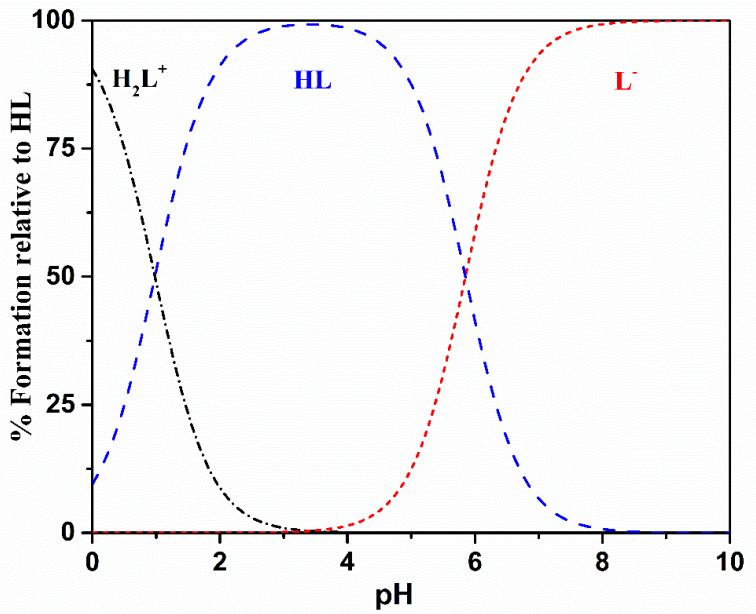

Fig. S10. Distribution diagram of TT9, calculated using the equilibrium constants reported in Table 3 of the typescript.

Based on the distribution diagram of Fig. S10, the clear isosbestic point at λ=313 nm in the collection of spectra of Fig. S8, is related with the equilibrium between the neutral and deprotonated forms of TT9, *i. e.* $HL + H_2O \rightleftarrows H_3O^+ + L^-$.

The UV-VIS spectra, at constant total concentration and different pH, are reported in Fig. S11 for the system Cu(II)/TT9.

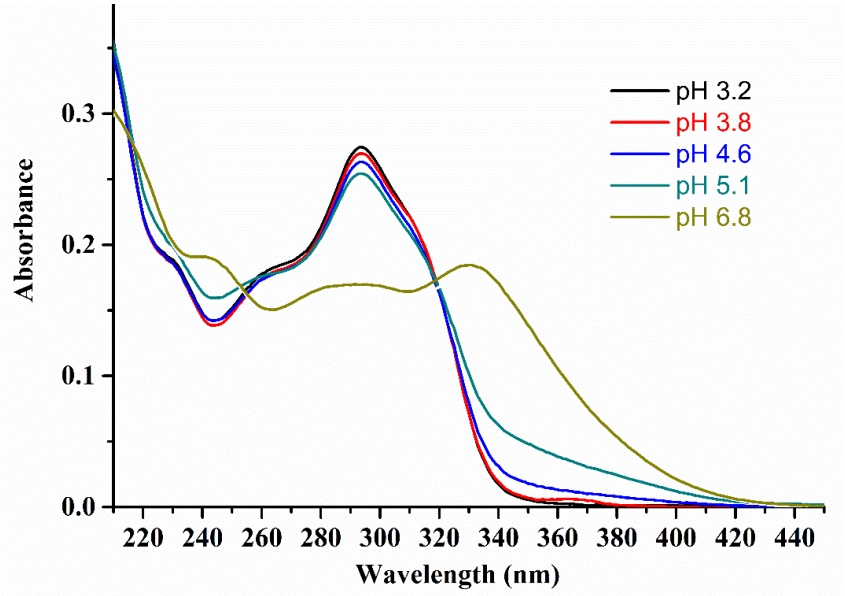

Fig. S11. UV−VIS absorption spectra of the system Cu(II)/TT9 at constant total concentration C_L = 3.0×10^{-5} M of the ligand and C_M = 6.0×10^{-5} M of the metal, in NaCl 0.5 M/ethanol 4% (v/v) recorded at 3 <pH <7.

In Fig. S12 are reported the Absorbance (at λ constant) *vs* pH experimental data at two different wavelengths. The experimental data were interpreted by the HYPERQUAD program in order to get the conditional stability constants of the complexes reported in Tab. 4 of the typescript.

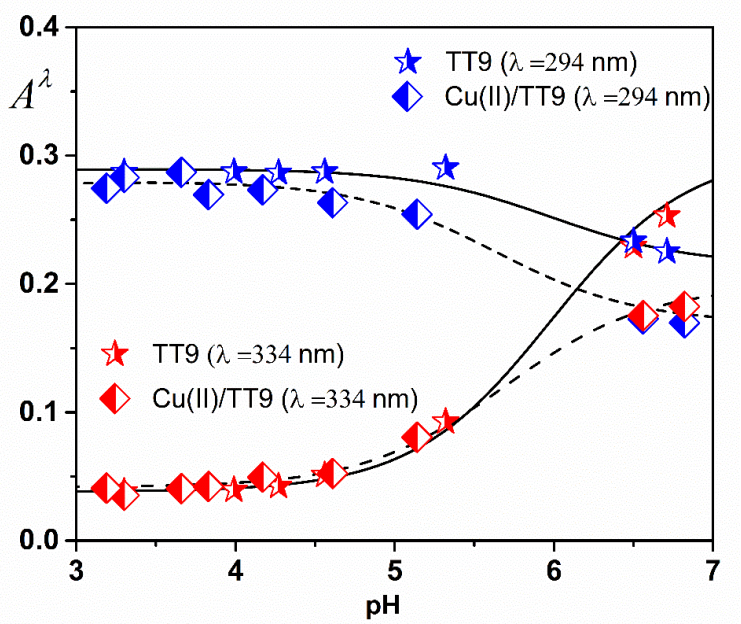

Fig. S12. UV-VIS titration curves of Cu(II)/TT9, at two different wavelengths. The experimental points, (Absorbance/pH) at two fixed wavelengths are taken from Fig. S11 and are represented by blue and red squares. The points are fitted with the continuous dashed lines, calculated using the Bouger-Lambert-Beer equation. The experimental points at the same wavelengths (blue and red stars) and the continuous solid curves for the system only containing TT9 are also reported for comparison.

The distribution diagram of the system Cu(II)/TT9, calculated using the conditional stability constants reported in Tab. 4 of the typescript, is shown as Fig. 11 of the typescript. Again, based on the distribution diagram of Fig. 11 of the typescript, the clear isosbestic point at λ=320 nm in the collection of spectra of Fig. S11, is related with the equilibrium between the two complexes $Cu(HL)^{2+}$ and CuL^{+}, *i. e.* $Cu(HL)^{2+} + H_2O \rightleftarrows CuL^{+} + H_3O^{+}$. It is interesting to determine the equilibrium constant K'_{a2} of the latter reaction, because it gives indication on the acidity of the coordinated free ligand, and can be compared with K_{a2}, that is related to the acidity of the free neutral ligand.

Now, indicating

$$A = Cu^{2+} + HL \rightleftarrows Cu(HL)^{2+} \quad \beta_1$$

$$B = Cu^{2+} + L^{-} \rightleftarrows Cu(L)^{+} \quad \beta_2$$

$$C = HL + H_2O \rightleftarrows H_3O^{+} + L^{-} \quad K_{a2}$$

$$D = Cu(HL)^{2+} + H_2O \rightleftarrows CuL^{+} + H_3O^{+} \quad K'_{a2}$$

It is evident that

$$D = B - A + C$$

So, it is

$$K'_{a2} = \frac{\beta_2 \cdot K_{a2}}{\beta_1}$$

And, therefore,

$$pK'_{a2} = -log\beta_2 + pK_{a2} + log\beta_1$$

In Fig. S13 is reported the plot of the calculated molar extinction coefficients for the system Cu(II)/HL.

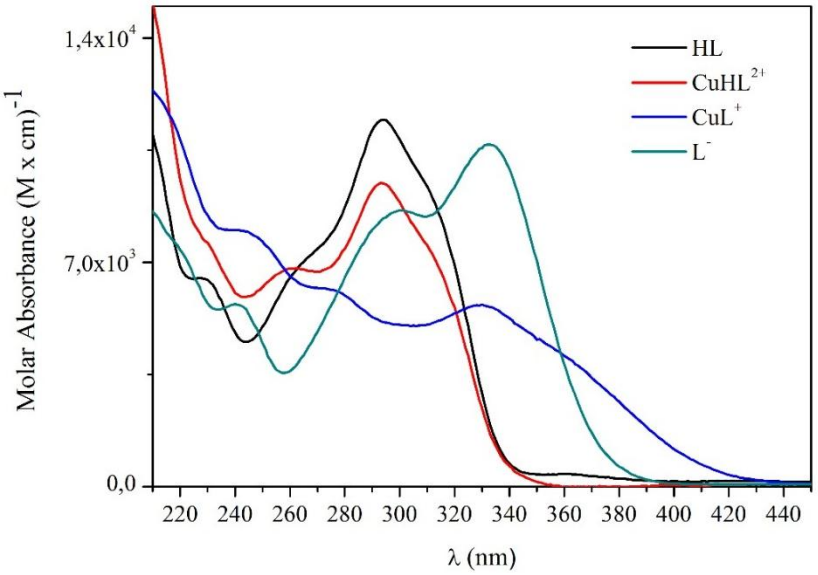

Fig. S13. Calculated molar extintion coefficients for the various species present in the system Cu(II)/HL.

The UV-VIS spectra, at constant total concentration and different pH, are reported in Fig. S14 for the system Zn(II)/TT9.

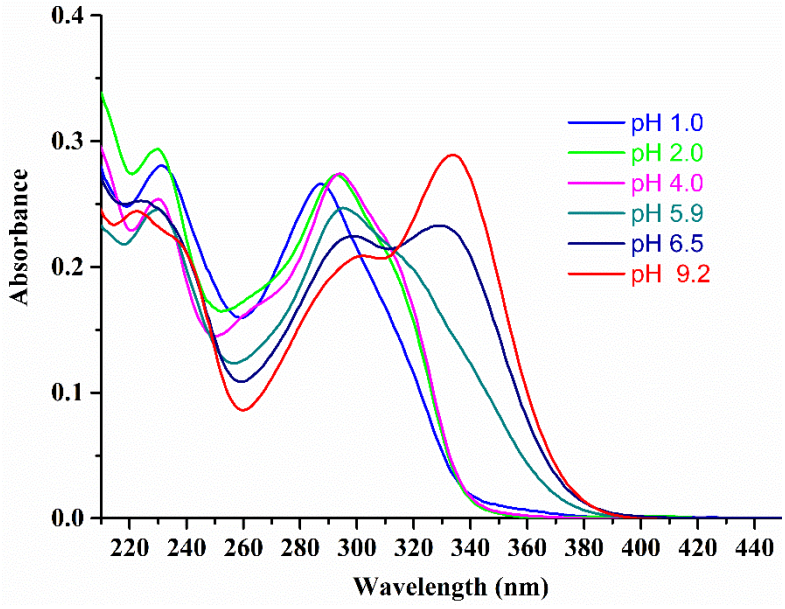

Fig. S14. UV−VIS absorption spectra of the system Zn(II)/TT9 at constant total concentration C_L = 3.0×10^{-5} M of the ligand and C_M = 3.0×10^{-5} M of the metal, in NaCl 0.5 M/ethanol 4% (v/v) recorded at 1 <pH <10.

In Fig. S15 is reported the distribution diagram of the system Zn(II)/TT9, calculated using the conditional stability constants reported in Tab. 4 of the typescript.

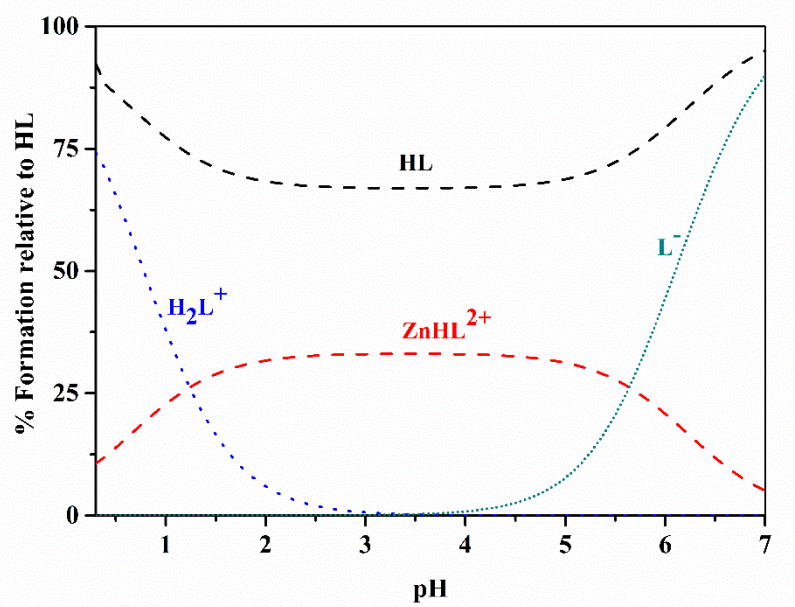

Fig. S15. Distribution diagram of the system Zn(II)/TT9, calculated using the equilibrium constants reported in Tables 3 and 4 of the typescript.

In Fig. S16 is reported the plot of the calculated molar extiction coefficient for the system Zn(II)/HL.

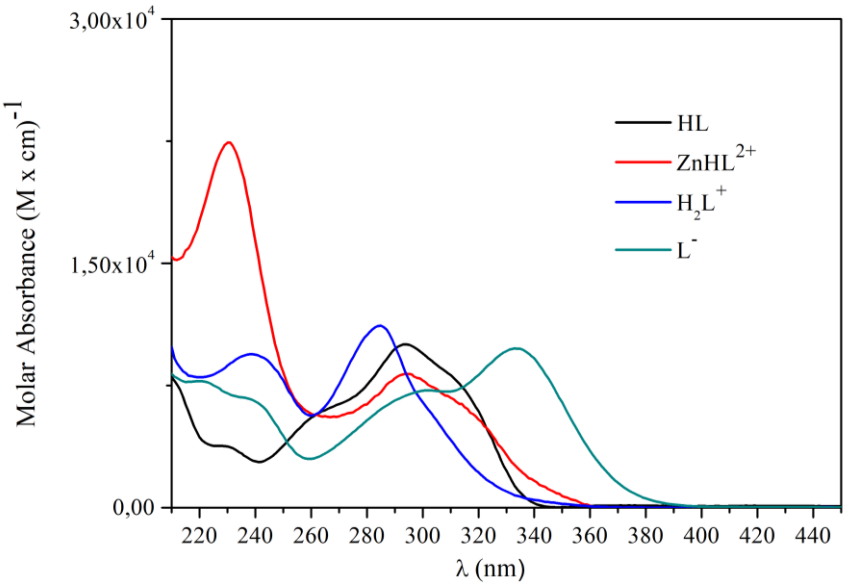

Fig. S16. Calculated molar extintion coefficients for the various species present in the system Zn(II)/HL.

Crystal packing

The crystal packing of TT9·H_2O, shown in Fig. S17, is of layered type.

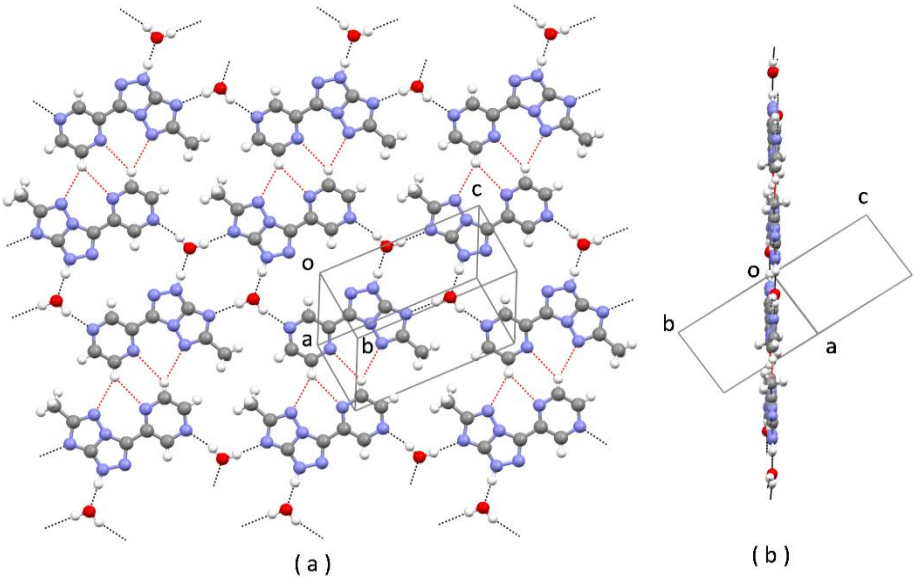

Fig. S17. Crystal packing of TT9·H_2O; (a) front view of a planar layer; (b) edge view of the same layer.

Molecules are arranged in planar ribbons through strong H-bonds involving N2-H donor and N3 and N6 acceptors of the triazolo-triazole molecule and water molecules. Tetramolecular ring-patterns $R_4^4(12)$ and $R_4^4(18)$ are formed. The ribbons are linked between each other through weak H-bonds involving bifurcated C4-H donor and N4 and N7 acceptors, in such a way that only one strong acceptor (N1) is not directly involved in the H bonding patterns. In this way, infinite planar layers are formed (Fig. S17(b)). The layers are parallel to the lattice planes $\bar{1}2\bar{2}$, and this is consistent with $\bar{1}2\bar{2}$ being the most intense reflection of the whole diffraction pattern. The stacking distance between the planes is rather short, $d_{\bar{1}2\bar{2}}$ = 3.247 Å, a feature that can be considered typical of layered structures formed by N-rich compounds.[5]

The crystal packing of TT9·HCl is shown in Fig. S18.

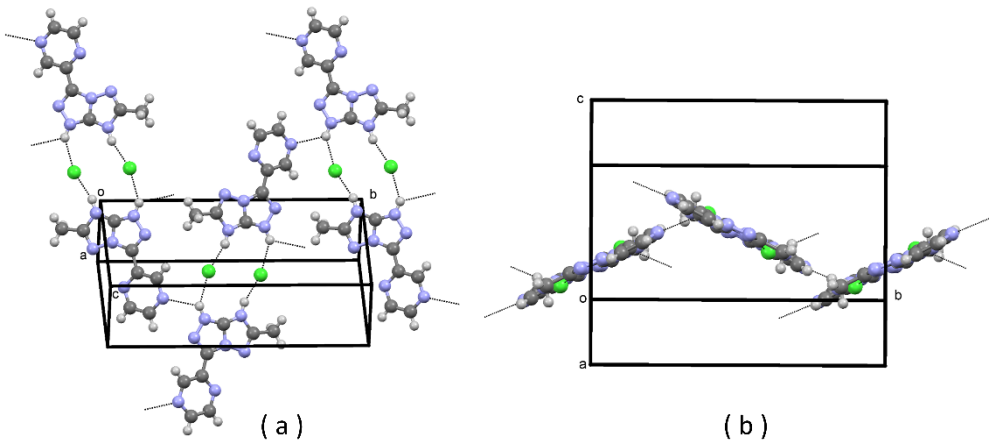

Fig. S18. Partial crystal packing of TT9·HCl. (a) face view; (b) edge view.

Organic cations and chloride anions form cyclic tetrameric motifs, $R_4^2(12)$. The motifs are held by strong H bonds between N2-H/N3-H donors and chloride acceptors, and are placed in a zig-zag arrangement along *b*.

The crystal packing of $NaC_8H_6N_7$ trihydrate is shown in Fig. S19.

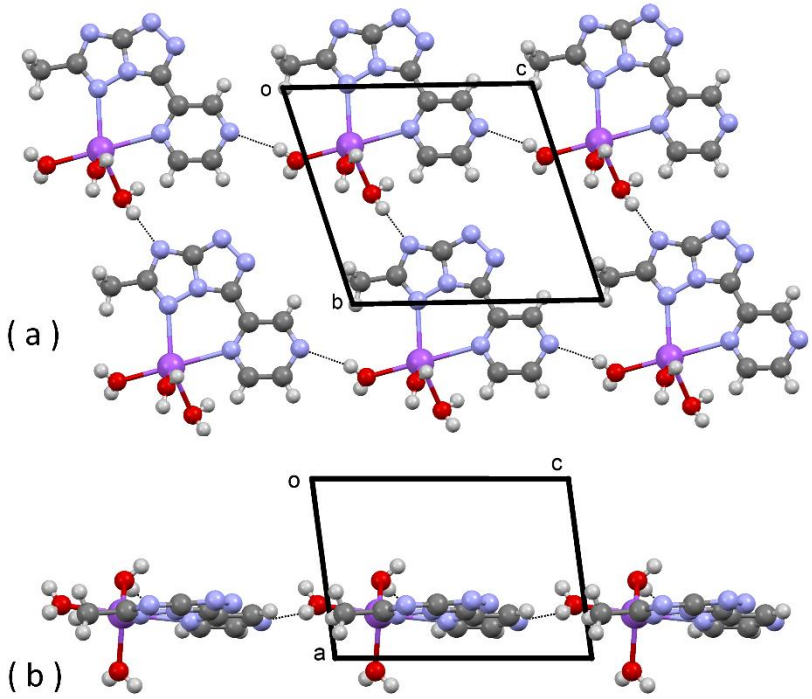

Fig. S19. Partial crystal packing of $NaC_8H_6N_7$ trihydrate.

The crystal structure is characterized by a complex pattern of strong H-bonds, involving N acceptors of triazolo-triazolate and O atoms of water molecules, and donor O-H atoms of water molecules. Apart from N4 and N6, which are coordinated the the metal cation, and N5, all N atoms of the organic anion are involved in strong H bonds. Tetramolecular ring patterns are evident in Fig. S19(a). Layers of H-bonded molecules, parallel to the crystallographic planes with Miller indices 200, are piled up along *a*, with spacing $d_{200} = 3.39$ Å, as shown in Fig. S19(b).

Apoptosis Assay

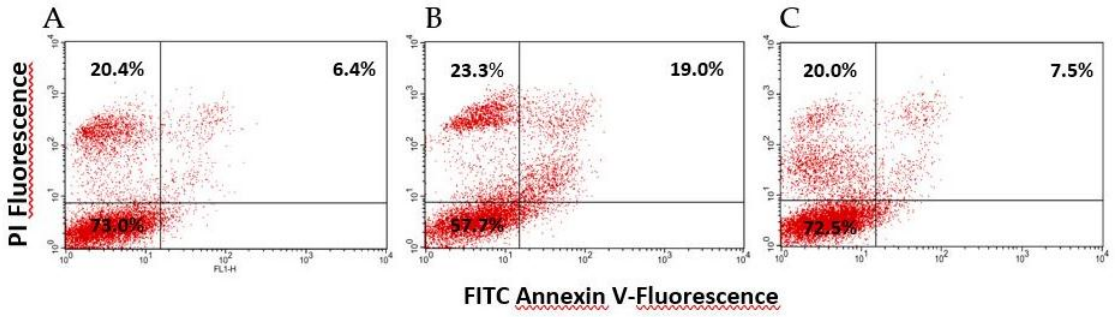

Fig. S20. Apoptosis analysis with annexin V-FITC and PI double staining on HeLa cells. Annexin V is used to specifically identify cells in early and advanced apoptosis stage, PI is used to stain both advanced apoptotic and necrotic cells. HeLa were seeded at 50.000 cells/well on 6-well plate and treated with 50 µM of molecules for 48 h. Panel A: control (vehicle treated cells); Panel B: cells treated with TT9, Panel C: cells treated with TT4. Lower left quadrant: viable cells; upper left: necrotic cells; upper right + low right: advanced + early apoptotic cells. These pictures are representative of two independent experiments.

Material and Methods

Apoptosis Assay

To perform apoptosis analysis, HeLa cells were seeded at 5x104 cells/mL density in a 6–well plate. After 24 h incubation, the cells were treated with the examined compounds or vehicle and incubated at 37 °C. Apoptosis was analyzed after 48h by double staining with annexin V/FITC and propidium iodide (PI) (eBioscience, USA) [6]. The cell undergoing apoptosis was measured and quantified using a flow cytometer equipped with a 488 nm argon laser (Becton Dickinson, USA) by Cell Quest software. All FACS analyses were performed at least 2 times.

References

[1] J. Senthilnathan, C.-C. Weng, J.-D. Liao and M. Yoshimura, *Sci. Rep.*, 2013, **3**, Article number: 2414.

[2] G. Biedermann and L. G. Sillén, *Ark. Kemi.* 1953, **40**, 425-440.

[3] G. Gran, *Analyst* 1952, **77**, 661–671.

[4] P. Gans, A. Sabatini and A. Vacca, *Talanta* 1996, **43**, 1739-1753.

[5] R. Centore, M. Causà, S. Fusco and A. Carella, *Cryst. Growth Des.*, 2013, **13**, 3255-3260.

[6] D. Capasso, S. Di Gaetano, V. Celentano, D. Diana, L. Festa, R. Di Stasi, L. De Rosa, R. Fattorusso and L. D. D'Andrea, *Molecular BioSystems*, 2017, **13**(8), 1619-1629.